Excerpt from the Proceedings of the 2011 COMSOL Conference in Stuttgart

Combined Analytical and Numerical Modeling of a Resonant MEMS Sensor for Viscosity and Mass Density Measurements

S. Cerimovic[*,1], R. Beigelbeck[2], H. Antlinger[3], J. Schalko[1,2], B. Jakoby[3], F. Keplinger[1]
[1]Institute of Sensor and Actuator Systems, Vienna University of Technology, Vienna, Austria
[2]Institute for Integrated Sensor Systems, Austrian Academy of Scien., Wr. Neustadt, Austria
[3]Institute for Microelectronics and Microsensors, Johannes Kepler University, Linz, Austria
*Corresponding author: Gußhausstr. 27-29, A-1040 Vienna, Austria, samir.cerimovic@tuwien.ac.at

Abstract: A resonant MEMS sensor for viscosity and mass density measurements of liquids was modeled. The device is based on Lorentz-force excitation and features an integrated piezoresistive readout. The core sensing element is a rectangular vibrating plate suspended by four beam springs. Through a conductive layer on the beam springs a sinusoidal excitation current is driven. In the field of a permanent magnet, the Lorentz-force excites time-harmonic plate vibrations. Evaluating the characteristics of the resonant system allows estimation of viscosity and mass density of the liquids. In this paper, we present a semi-numerical simulation approach that combines advantages of analytical and FEM modeling. This combination reduces required computing power and memory capacity. The good agreement between measured and simulated results indicates that such simulations are a convenient method to predict the sensor characteristic and to support the sensor design.

Keywords: MEMS, viscosity, mass density, Lorentz-force, piezoresistive readout

1. Introduction

Monitoring of viscosity and mass density of liquids is mandatory in many industrial applications. By detecting spurious variations and implementing feedback loops the process quality can be maintained. Typical laboratory instruments for viscosity measurement impose shear deformations in the liquid and measure the associated externally applied shear force [1]. Most often, rotational movements of cylinders or cones are utilized. Sample preparation for such devices is time-consuming and error-prone. Moreover, due to bulky mechanical parts they can not be sufficiently miniaturized. Thus, for online monitoring applications miniaturized devices such as thickness shear mode (TSM) resonators [2] or micro-electro-mechanical systems (MEMS) structures like vibrating beams [3] or cantilevers [4] offer some decisive advantages.

The presented sensor for viscosity and density measurements is based on MEMS technology and is suitable for integration in online monitoring systems. The core sensing element is a rectangular vibrating plate suspended by four beam springs [5]. The Lorentz-force excited plate vibrations are damped by the liquid under test. By evaluating the characteristics of the resonant system, it is possible to extract viscosity and mass density of the liquid.

The sensor design was supported by FEM modeling. A 3D-model of the sensor was developed in order to investigate the influence of design variations on the sensor behavior and to find the optimal geometry of the sensor elements. Finally, the reliability of the model was verified by comparing the laboratory measurements with the simulations results.

2. Sensor Device

The schematic of the sensor device is depicted in Fig. 1. The rectangular silicon plate measures 100×100×20 µm³ whereas each supporting beam spring is 5 µm wide and 20 µm high. The length l_{spring} of the beams was subjected to FEM simulations. Values in the range of 150 to 750 µm were considered. The silicon beams bear a conductive metal layer consisting of 80 nm thin titanium and 570 nm thin gold films. In the field of a permanent magnet (flux density $\boldsymbol{B} = -320\,\mathrm{mT}\cdot\mathbf{i}_z$), the imposed sinusoidal current $i_e(t)$ excites lateral deflections of the springs leading to time-harmonic in-plane oscillations of the suspended plate.

The ends of two beam springs are forked. One prong carries the metal layer for the excitation current while the other consists of a piezoresistive element (R_3 and R_4, respectively). The resistor dimensions are 50×5×20 µm³ with a typical electric resistance of a few kΩ. These resistors accompanied with two additional resistors placed on the silicon rim (R_1 and R_2) form a half Wheatstone bridge. Due to plate vibrations, the piezoresistors R_3 and R_4 are subjected to either compressive or tensile stress. This changes their electric

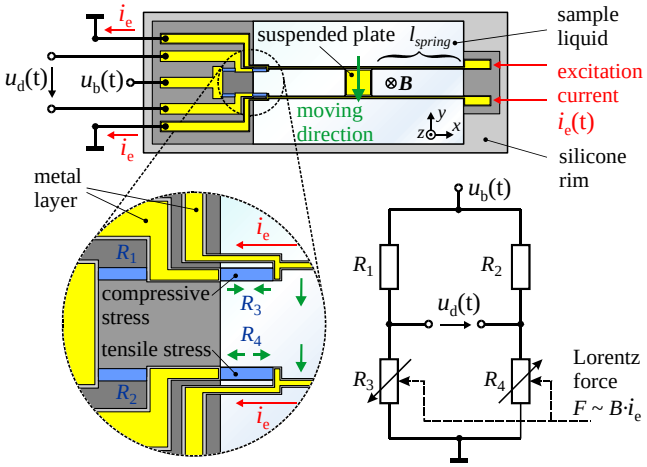

Figure 1. Schematic of the sensor device illustrating suspended plate and piezoresistive readout. The plate vibrations are excited by the Lorenz force. The piezoresistors $R_{1\text{-}4}$ form a Wheatstone bridge supplied by the voltage u_b. The resistors R_3 and R_4 are subjected to alternating compressive and tensile stress due to the plate deflection.

resistance resulting in a bridge unbalance. As output signal we analyze the differential voltage $u_d(t)$.

3. Modeling

Without the liquid load the vibrating structure can be modeled very efficiently by solely using the undamped solid-stress-strain-mode of COMSOL multiphysics. The frequency response analysis yields the resonant frequency as a characteristic parameter of the system. Immersing the sensor in a liquid shifts the resonant frequency towards lower values, depending on the viscosity and mass density of the liquid. The accurate FEM modeling of the sensor behavior requires Navier-Stokes-mode for the subdomain with the liquid. Owing to the high aspect ratio of some sensor elements and the large dimensions of the additional fluid subdomain compared to the resonant structure, this approach results in high memory and CPU usage. Thus, pure numerical simulations utilizing finite element method are inappropriate in this case. On the other hand, simplified analytical modeling yields results deviating up to 30% from the measured values [6]. Therefore, we propose a semi-numerical approach that combines advantages of analytical and numerical modeling.

Figure 2 shows the geometry of the 3D-FEM model. In order to reduce the number of mesh elements, the silicone rim with the additional piezoresistors is omitted. Dimensions of the model elements agree with the values specified in the sensor design chapter. The model involves two application modes. The conductive-media-mode calculates the current distribution in the conductive layer on the top of the springs and plate (violet colored area in inset of Fig. 2). For this

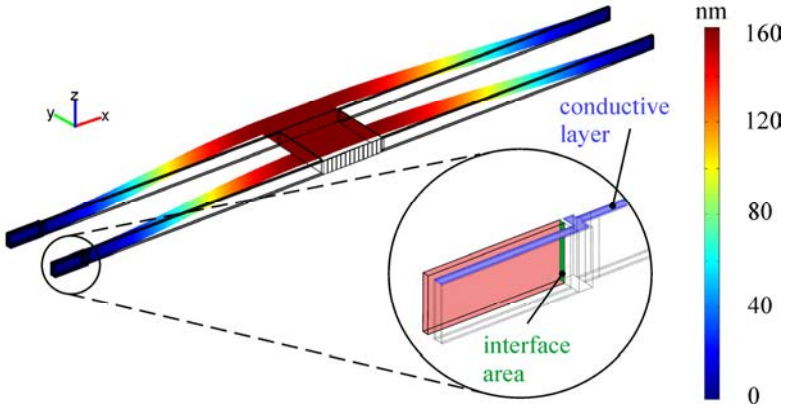

Figure 2. Geometry of the 3D-FEM model. The color-bar indicates the displacement amplitude in *y*-direction at resonant frequency when using air as fluid. The inset shows the forked end of one spring with the piezoresistor (highlighted area) and the interface area where the stress was evaluated.

purpose, the boundary condition of the conductive layer on the right side is set to imposed current density and on the left side to the ground. This corresponds to the schematic representation in Fig. 1. All other boundaries in this mode are set to electric insulation.

The second application mode is the solid-stress-strain mode. Here, the results from the first mode are used to impose the acting Lorentz-force on the vibrating structure. The body load (force/volume) for the conductive layer in the second mode is set to

$$\begin{aligned} F_x &= -J_{\text{y\_emdc}} \cdot B, \\ F_y &= J_{\text{x\_emdc}} \cdot B, \\ F_z &= 0, \end{aligned} \tag{1}$$

where $J_{\text{x\_emdc}}$ and $J_{\text{y\_emdc}}$ are current densities in the conductive layer calculated by the first application mode (emdc) and $B = 320$ mT is the used magnetic flux density. All other subdomains in this mode are unloaded. The liquid-structure interaction is implemented as additional mass and damping to the springs and the plate. The required parameters are gained through an analytical model of the rectangular vibrating cantilever [7]. The model is valid if the vibration amplitudes are far smaller than the beam geometry, the surrounding liquid is assumed to behave incompressible, the beam cross-section is uniform over the entire length, and the beam length greatly exceeds its nominal width. These requirements are all fulfilled in our case.

To account for interaction of the four sensor springs with the surrounding liquid, the hydrodynamic function $\Gamma(\omega)$ must be calculated at first. The exact analytical result for $\Gamma(\omega)$ for a beam with a circular cross-section is given by

$$\Gamma_{\text{circ}}(\omega) = 1 + \frac{4\mathrm{j}K_1\left(-\mathrm{j}\sqrt{\mathrm{jRe}}\right)}{\sqrt{\mathrm{jRe}}K_0\left(-\mathrm{j}\sqrt{\mathrm{jRe}}\right)}, \tag{2}$$

where $\mathrm{j} = \sqrt{-1}$ is the imaginary unit, $\mathrm{Re} = \rho\omega h^2/(4\eta)$ is the related Reynolds number, and K_0 and K_1 are the modified Bessel functions of the third kind. The density and viscosity of the liquid are denoted by ρ and η, respectively. Furthermore, ω is a characteristic angular frequency of the vibration and $h = 20$ µm is the height of the cantilever beam. The rectangular cross-section of the sensor springs can be taken into account by multiplying Eq. 2 with an appropriate correction function $\Omega(\omega)$ as follows

$$\Gamma_{\text{rect}}(\omega) = \Gamma_{\text{circ}}(\omega)\,\Omega(\omega). \tag{3}$$

The exact expression of the complex function $\Omega(\omega)$ is stated in [7]. Using the hydrodynamic function, we can now calculate the added mass per unit length of the springs due to liquid loading [6]

$$m'_{\text{a,spring}} = \rho\frac{\pi}{4}h^2\Gamma', \tag{4}$$

where Γ' is the real part of the hydrodynamic function $\Gamma_{\text{rect}}(\omega)$. Note that the added mass is frequency dependent. Finally, the mass density of the springs used for the simulations reads

$$\rho_{\text{spring}} = 2330\frac{kg}{m^3} + \frac{m'_{\text{a,spring}} \cdot l_{\text{spring}}}{V_{\text{spring}}}. \tag{5}$$

$V_{\text{spring}} = A_{\text{spring}} \cdot l_{\text{spring}}$ denotes beam volume, where $A_{\text{spring}} = 5\times20$ µm² is the beam cross-section area.

With respect to its large lateral surface, the springs vibrate out-of-plane. Such a vibration mode generates a velocity field in the liquid that is associated with high damping. This damping is accounted for by using a Rayleigh damping model where the mass damping parameter α is set to zero and the stiffness damping parameter is given by

$$\beta_{\text{spring}} = \frac{\gamma}{k} = \left(\gamma'_{\text{a,spring}} \cdot L\right) \cdot \frac{L^3}{32w^3hE}. \tag{6}$$

Here, γ denotes the viscous damping coefficient and $E = 169$ GPa is the Young's modulus of silicon in [110] direction [8]. In Eq. 6 two supporting springs forming one side of the H-shaped sensor are modeled as one long doubly-clamped, uniformly loaded beam cantilever with a spring constant of $k = 32w^3hE/L^3$, where $w = 5$ µm is the cantilever width and $L = 2 \times l_{\text{spring}}$ is the total cantilever length. The added damping coefficient per unit length of the springs $\gamma'_{\text{a,spring}}$ can be calculated using the imaginary part of the hydrodynamic function Γ''

$$\gamma'_{\text{a,spring}} = \rho\frac{\pi}{4}h^2\omega\Gamma''. \tag{7}$$

Contrary to the springs, the suspended plate vibrates in an in-plane mode. Thus, mainly shear waves associated with a low damping of the plate are excited in the surrounding liquid. It can be shown [6] that the major part of additional mass and damping due to liquid interaction stems from the vibrating springs. Therefore, we only consider the front face of the rectangular plate which vibrates in an out-of-plane mode (hatched area in Fig. 4) and use Eq. 4 multiplied with a plate length to calculate its additional mass density. For reasons of simplification, all other effects that

influence the plate added mass as well as the added damping of the plate are neglected. Moreover, the conductive metal layer is modeled as 650 nm thick solely gold film, i.e., the influence of titanium is also neglected. The boundary conditions in the solid-stress-strain mode are set to fix at the ends of the beam springs and to free for the rest.

The sensor is fabricated on a silicon-on-insulator (SOI) wafer. The 20 µm thick device layer is p-doped silicon which is inherently piezoresistive. The sensor utilizes this effect for the readout of the plate deflection. On the device layer the four piezoresistors are aligned in the [110] direction. In this case, the change of the resistance due to applied stress reads

$$\Delta R = \pi_l \sigma_l R_0, \tag{8}$$

where R_0 is the resistance at zero stress and the longitudinal piezoresistance coefficient amounts to $\pi_l = 71.8 \cdot 10^{-11}$ Pa^{-1}. The longitudinal stress σ_l is calculated by evaluating the average force in x-direction at the interface between the piezoresistor and the spring (indicated in the inset of Fig. 2). We record both the frequency response of the amplitude and the phase of ΔR. The resistance change ΔR is directly proportional to the bridge output u_d which is evaluated in the experimentally setup.

4. Results

First, the impact of geometry variations on the resonant frequency of the scarcely-damped (i.e., in air vibrating) system is investigated. Experimentally, the plate deflection is measured with a common micro system analyzer, whereas in COMSOL the frequency response analysis of the solid-stress-strain mode is used. With decreasing beam length the resonant frequency shifts to higher values. This is particularly important if so called Maxwellian liquids are measured. Contrary to the Newtonian liquids, the measurement results depend on the vibrating frequency of the probe. Thus, the possibility to sense the viscosity in a wide frequency range is inevitable, if the full rheological behaviour of a liquid is of interest. We fabricated five sensor embodiments with 150, 300, 450, 600, and 750 µm beam length and compared their in-air-vibrating resonant frequency with the simulation values. Figure 3 shows a photo-micrograph of a sensor embodiment with 600 µm beam length.

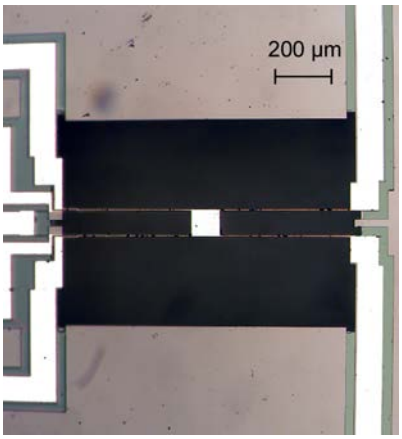

Figure 3. Photomicrograph of a suspended plate sensor embodiment with 600 µm beam length.

The comparison of measured and simulated results is illustrated in Fig. 4. The resonant frequencies of the five sensor embodiments differ in the range of about one decade. The best agreement with the measured results demonstrates the sensor with the shortest length of the beams, where the relative error amounts to only 2%. With increasing beam length, the relative error becomes higher and reaches the value of 35% for the senor with 750 µm beams. One reason for this deviation is the spurious underetching of the silicon structures arising from the deep reactive-ion etching (DRIE) process, during the sensor fabrication. Moreover, the possible intrinsic stress of the vibrating structure is also not considered. These effects primary affect the beams rather than the plate and are, hence, more emphasized by the sensors with longer beams. Nevertheless, the FEM simulations proved to be a suitable tool to predict the frequency range of the sensors, which is of particular importance for the sensor design.

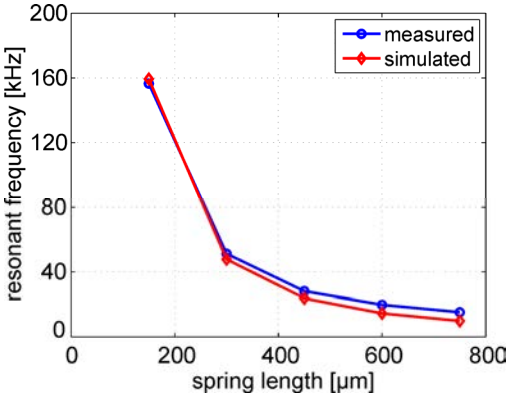

Figure 4. Dependence of resonant frequency on the length of the springs l_{spring} for sensor operation in air.

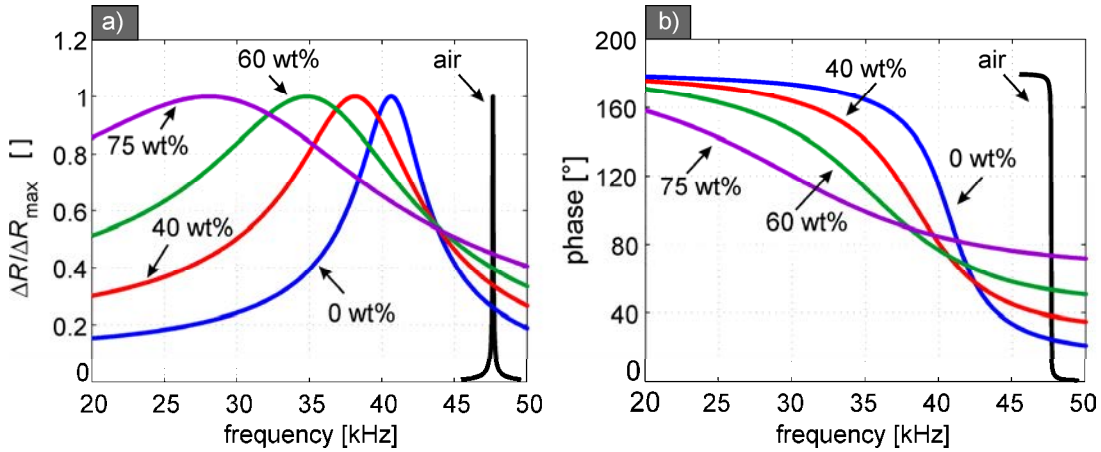

Figure 5. Simulated relative amplitude and phase of the resistance change ΔR as a function of the excitation current frequency. For the simulation, air and different glycerol-water mixtures were considered. The spring length of the sensor was set to 300 µm.

Next, we investigate the influence of the liquids on the resonant behavior of the system. Here, glycerol-water mixtures are chosen as test liquids because they are inexpensive, non-toxic, easy to handle, and feature a well-defined dependence between glycerol concentration, mass density, and viscosity. However, the sensing principle is not limited to glycerol-water mixtures and, therefore, the device can be utilized for viscosity and density monitoring of arbitrary liquids in the viscosity range of up to 100 mPas. For this investigation, a sensor with 300 µm spring length is simulated and subsequently experimentally characterized. In the laboratory, the frequency of the bridge excitation current i_e is swept and the bridge voltage u_d evaluated (Fig. 1). More details about measurement setup can be found in [9]. In COMSOL, we use again the frequency response analysis recording ΔR (see Eq. 8). The highest resonant frequency and quality factor can be achieved when the device is operated in air (i.e., approximately no viscous damping). When the sensor is immersed in the sample liquids, the resonant frequency f_r shiftes to the lower values and the damping factor D increases depending on the mass percentage of glycerol (i.e., the viscosity and the mass density of the mixture, Fig. 5).

In order to estimate the damping factor, we assume that the resonant system can be approximated by a second order behavior and fitt the amplitude response

$$\Delta\hat{R}(f) = \left| \frac{A_0}{1 + \mathrm{j}\cdot 2D\cdot\frac{f}{f_0} - \frac{f^2}{f_0^2}} \right| \qquad (9)$$

to the results. In Eq. 9, A_0 represents the output signal at static plate deflection ($f = 0$ Hz), D is the damping factor of the system, and f_0 is the natural resonant frequency of the system without damping ($f_r = f_0\sqrt{1-2D^2}$ is the frequency where ΔR reaches its maximum).

Figure 6 depicts simulation results for different glycerol-water mixtures in comparison with measured values. Whereas the trend of both characteristics is similar to the measured ones, the absolute values reveal the maximum deviation of about 15% for resonant frequency and below 20% for damping factor. The reason for that are numerous simplifications of the applied sensor model. Neither the measured nor the simulated sensor output can be exactly described by a system of second order as assumed for the fitting procedure (Eq. 9) in order to obtain the damping factor D. This mismatch increases with higher damping factor. Since the plate damping was totally neglected, the simulations generally yield a

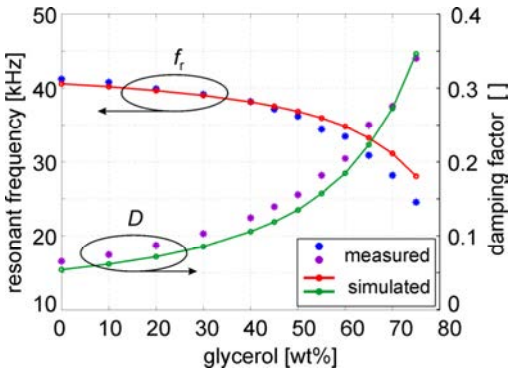

Figure 6. Dependence of the resonant frequency and the damping factor on the glycerol percentage of the mixtures. The spring length of the sensor was set to 300 µm.

smaller damping factor, except in the higher viscosity range (i.e., increasing glycerol percentage) where the damping factor estimation is more inaccurate. For precise modeling of the piezoresistive elements, the stress tensor and the piezoresistance matrix of silicon must be utilized over the whole volume of the piezoresistor, whereas we just use the longitudinal stress σ_l according to Eq. 8. Moreover, the influence of the ambient temperature (25°C) is only considered regarding the viscosity and density of the liquid under the test, whereas its impact on the mechanical properties of the sensor materials is neglected.

Despite the partly higher relative error, the simulations enable to get a glimpse of the trend of the output characteristics and to approximately estimate the resonant frequency and the damping.

5. Summary and Conclusion

Modeling of a resonant MEMS sensor suitable for monitoring of viscosity and mass density of liquids was presented. The device is based on Lorentz-force excitation and features an integrated piezoresistive readout. The core sensing element of the device is a rectangular, in-plane vibrating plate suspended by four beam springs which is damped by the liquid under test. Evaluating the properties of the resonant system allows the estimation of viscosity and mass density of the liquid.

The model involves two application modes. The first one calculates the current distribution in the conductive layer. These results are then used to impose the acting Lorentz-force on the vibrating structure. The liquid-structure interaction is implemented as additional mass and damping to the springs and the plate. The required parameters are gained utilizing an analytical model of the rectangular vibrating cantilever.

The combination of analytical and numerical modeling provides a convenient way to reduce computing power and memory capacity. The simulation results give the right trend of output characteristics for varied viscosity and help to estimate the resonant frequency and the damping. The model is also useful for the sensor design as the effects of various geometry variations can be studied qualitatively.

8. References

[1] B. Jakoby, R. Beigelbeck, F. Keplinger, F. Lucklum, A. Niedermayer, E.K. Reichel, C. Riesch, T. Voglhuber-Brunnmaier, B. Weiss, "Miniaturized sensors for the viscosity and density of liquids-performance and issues," I*EEE Transactions on Ultrasonics, Ferroelectrics and Frequency Control*, vol.57(1), pp.111-120 (2010)

[2] K.K. Kanazawa, J.G. Gordon, "Frequency of a Quartz Microbalance in Contact with Liquid", *Anal. Chem.*, vol.57, pp.1770-1771 (1985)

[3] C. Riesch, A. Jachimowicz, F. Keplinger, E.K. Reichel, B. Jakoby, "A Novel Sensor System for Liquid Properties Based on a Micromachined Beam and a Low-Cost Optical Readout", Proc. IEEE Sensors Conf., Atlanta, USA (2007).

[4] A. Agoston, F. Keplinger, B. Jakoby, "Evaluation of a vibrating micromachined cantilever sensor for measuring the viscosity of complex organic liquids", *Sensors and Actuators A*, vol.123-124, pp. 82-86 (2005)

[5] C. Riesch, E.K. Reichel, A. Jachimowicz, J. Schalko, B. Jakoby, F. Keplinger, "A micromachined suspended plate viscosity sensor featuring in-plane vibrations and integrated piezoresistive readout," Proc. TRANSDUCERS 2009, pp.1178-1181 (2009)

[6] C. Riesch, *"Micromachined Viscosity Sensors"*, Shaker Verlag, Aachen (2009).

[7] J. E. Sader, "Frequency response of cantilever beams immersed in viscous fluids with applications to the atomic force microscope", *J. Appl. Phys.*, vol.84, pp.64-76 (1998)

[8] M.A. Hopcroft, W.D. Nix, T.W. Kenny, "What is the Young's Modulus of Silicon? ", *J. Microelectromechanical Syst.*, vol.19(2), pp.229-238 (2010)

[9] S. Cerimovic, R. Beigelbeck, H. Antlinger, J. Schalko, B. Jakoby: "Viscosity and Density Measurements of Glycerol-Water Mixtures Utilizing a Novel Resonant MEMS Sensor"; Proc. SPIE Microtechnologies International Symposium, Prague, Czech Republic, 8066 80662E-1 (2011).

9. Acknowledgements

We gratefully acknowledge partial financial support by the Austrian Science Fund FWF (research grant L657-N16).